Electronic structure of the oxide-diluted magnetic semiconductor $Zn_{1-x}Mn_xO$

T. Mizokawa,[1] T. Nambu,[2] A. Fujimori,[1,2] T. Fukumura,[3] and M. Kawasaki[3]
[1]*Department of Complexity Science and Engineering, University of Tokyo, Hongo 7-3-1, Bunkyo-ku, Tokyo 113-0033, Japan*
[2]*Department of Physics, University of Tokyo, Bunkyo-ku, Tokyo 113-0033, Japan*
[3]*Institute for Materials Research, Tohoku University, Katahira 2-1-1, Aoba-ku, Sendai 980-8577, Japan*
(Received 26 February 2001; revised manuscript received 6 August 2001; published 8 February 2002)

We have studied the electronic structure of $Zn_{1-x}Mn_xO$ using photoemission spectroscopy measurements and configuration-interaction (CI) calculations on a MnO_4 cluster model. It is shown that the CI calculation can give a consistent description of the photoemission and *d-d* optical absorption spectra of $Zn_{1-x}Mn_xO$ as well as those of other II-VI- and III-V-based diluted magnetic semiconductors such as $Cd_{1-x}Mn_xTe$ and $Ga_{1-x}Mn_xAs$. The CI approach predicts that the magnitude of the *p-d* exchange constant in $Zn_{1-x}Mn_xO$ is much larger than that in $Ga_{1-x}Mn_xAs$.

DOI: 10.1103/PhysRevB.65.085209 PACS number(s): 75.50.Pp, 79.60.−i, 71.70.Gm

I. INTRODUCTION

In II-VI- and III-V-based diluted magnetic semiconductors (DMS) such as $Cd_{1-x}Mn_xTe$ and $Ga_{1-x}Mn_xAs$, $3d$ transition-metal ions are substituted for the cations of the host semiconductors.[1–3] The electronic structure of the substituted $3d$ transition-metal impurities in semiconductors is influenced by two competing factors: strong $3d$-host hybridization and strong $3d$-$3d$ Coulomb interactions. The strong Coulomb interaction between the $3d$ electrons is responsible for the multiplet structures observed in *d-d* optical absorption spectra. On the other hand, the hybridization between the transition-metal $3d$ and the host valence band gives rise to the magnetic interaction between the localized $3d$ spins and the carriers in the host valence band.[2] A configuration-interaction (CI) approach using a cluster model is a powerful tool to describe such systems in which the Coulomb interaction term and the hybridization term are competing. The electronic-structure parameters in the cluster model can be estimated by analyzing core-level and valence-band photoemission spectra of DMS. By using the obtained parameters as input, it is possible to estimate the magnitude of the magnetic interaction between the localized $3d$ spins and the carriers.

$Zn_{1-x}Mn_xO$ is a new class of DMS based on ZnO.[4] Since ZnO is transparent for visible light, a transparent magnet can be realized if $Zn_{1-x}Mn_xO$ exhibits ferromagnetism like III-V-based DMS such as $Ga_{1-x}Mn_xAs$ and $In_{1-x}Mn_xAs$.[5] In the III-V-based DMS, the Mn doping provides both the carriers and the localized spins. On the other hand, in $Zn_{1-x}Mn_xO$, the Mn doping gives only the localized spins and that the carrier concentration can be controlled independently by doping, e.g., Al. Since $Zn_{1-x}Mn_xO$ is expected to be one of the key materials for the spin-controlled semiconductor engineering, it is very interesting and important to investigate the electronic structure of $Zn_{1-x}Mn_xO$ and to compare it with those of $Cd_{1-x}Mn_xTe$ and $Ga_{1-x}Mn_xAs$. In this paper, we have studied the electronic structure of $Zn_{1-x}Mn_xO$ using photoemission spectroscopy and CI cluster-model analysis. We compare $Zn_{1-x}Mn_xO$ with the other DMS and give a CI description of the Mn impurities in ZnO, ZnS, ZnSe, ZnTe, and GaAs.

II. EXPERIMENT

$Zn_{1-x}Mn_xO$ thin films ($x=0.07$ and $x=0.13$) with Al dopant were prepared by pulsed-laser deposition on $ScAlMgO_4$ (001) substrates as reported in the literature.[4] X-ray-diffraction measurements confirm that the thin films have the wurtzite structure without impurity phase. An electron probe microanalysis shows that Mn ions are homogeneously distributed in the films. The Mn content is estimated by inductively coupled plasma atomic emission spectroscopy. By using Hall effect measurement, the carrier density is estimated to be 1.4×10^{20} cm^{-3} for $x=0.13$ and 2.9×10^{19} cm^{-3} for $x=0.07$.

Photoemission measurement was performed at BL-18A of Photon Factory, High Energy Accelerator Research Organization. All the data were taken in an ultrahigh vacuum below 10^{-10} Torr at room temperature. The valence-band spectra have been taken using synchrotron radiation. The total resolution including the monochromator and the electron analyzer was estimated to be about 200 meV from the Fermi edge of Ta wire in contact with the samples. We chose the Zn $3d$ peak as a reference for the binding energy (E_B) alignment [the Zn $3d$ peak in ZnO being located at $E_B=8.8$ eV from valence-band maximum (VBM)].[6] Core-level photoemission spectra were taken using the Mg $K\alpha$ source ($h\nu=1253.6$ eV). The resolution was ~0.8 eV estimated from the Au $4f$ core-level spectrum. Photoelectrons were collected using a VG CLAM hemispherical analyzer in the angle-integrated mode. In order to keep the sample surfaces clean, we repeated Ar-ion sputtering (1 kV) and annealing at 250 °C. The annealing had to be done at that low temperature to prevent Al_2O_3 segregation. We could not observe low-energy electron-diffraction patterns of 1×1 probably because of the temperature constraint. However, the valence-band spectrum taken at 45 eV is very similar to those reported for the clean ZnO surface,[6,7] indicating that the surface quality is reasonably good. The Mn content estimated from the Mn core-level intensity agreed with the bulk values within the error bar of 20%.

III. CONFIGURATION-INTERACTION APPROACH

The Mn impurities substituted for the cations in the II-VI and III-V semiconductors are tetrahedrally coordinated by

the anions and can be described by the MnY_4 cluster model (Y is an anion). In the cluster models, the $3d$-$3d$ Coulomb interaction and the $3d$-anion hybridization are taken into account and their strengths are treated as adjustable parameters. In the CI framework, the wave functions of the ground state and charge-conserving excited states, which we call N-electron states, are given by linear combinations of the d^n, $d^{n+1}\underline{L}$, . . . , $d^{10}\underline{L}^{10-n}$ configurations. Here, $\underline{L}$ denotes a hole in an anion p orbital. The anion-to-$3d$ charge-transfer energy is defined by $\Delta \equiv E(d^{n+1}\underline{L}) - E(d^n)$ and the $3d$-$3d$ Coulomb interaction energy by $U \equiv E(d^{n-1}) + E(d^{n+1}) - 2E(d^n)$, where $E(d^{n'}\underline{L}^{m'})$ is the center of gravity of the $d^{n'}\underline{L}^{m'}$ multiplet. These definitions make clear the chemical trends of the parameters.[8] It is also possible to define the charge-transfer energy $\Delta_{\rm eff}$ and the Coulomb interaction energy $U_{\rm eff}$ with respect to the lowest term of each multiplet. The multiplet splitting is expressed using Racah parameters B and C, which were fixed at the free ion values of Mn^{2+} ($B=0.119$ eV and $C=0.412$ eV). For Mn^{2+}, $\Delta_{\rm eff} = \Delta + (70B - 35C)/9 + 7C$ and $U_{\rm eff} = U + (14B - 7C)/9 + 14B + 7C$.

In the tetrahedral cluster model, one-electron transfer integrals between the $3d$ orbitals and the anion p orbitals are given by $(pd\sigma)$ and $(pd\pi)$: $T_{t2} \equiv \langle t_2|H|L_{t2}\rangle = \sqrt{4/3(pd\sigma)^2 + 8/9(pd\pi)^2}$ and $T_e \equiv \langle e|H|L_e\rangle = 2\sqrt{6}/3(pd\pi)$, where L_{t2} and L_e are ligand orbitals with T_2 and E symmetry of the T_d point group, respectively.[8] Here, the ratio $(pd\sigma)/(pd\pi)$ is fixed to -2.16.[9] In order to reproduce the photoemission, inverse photoemission, and d-d optical absorption spectra of II-VI DMS such as $Cd_{1-x}Mn_xTe$, the transfer integrals should be renormalized depending on the number of $3d$ electrons.[8] For example, the transfer integrals between d^{n-1} and $d^n\underline{L}$ are smaller by 20% and those between d^{n+1} and $d^{n+2}\underline{L}$ larger by 20% than those between d^n and $d^{n+1}\underline{L}$. The present calculation follows this prescription to renormalize the transfer integrals. In this paper, values for the d^n-$d^{n+1}\underline{L}$ transfer integrals are presented.

IV. RESULTS AND DISCUSSION

A. Mn 2p core-level photoemission

The Mn $2p$ core-level spectrum for the $x=0.13$ sample is shown in Fig. 1. The broad peak at ~667 eV is due to Mn $L_{2,3}M_{2,3}M_{4,5}$ Auger emission. The Mn $2p_{3/2}$ main peak has the satellite structure on the higher binding-energy side separated by ~6 eV. The Mn $2p$ core-level spectrum for $x=0.07$ (not shown) is nearly identical to that for $x=0.13$. The presence of the satellite structure allows us to analyze the spectrum using the MnY_4 cluster model and to extract the electronic-structure parameters Δ, U, and $(pd\sigma)$. The calculated result for $\Delta=6.5$ eV is shown by the solid curve in Fig. 1. In order to reproduce the photoemission spectra, the line spectra have been broadened by a Gaussian (representing the instrumental broadening and finite bandwidth effects) and a Lorentzian (lifetime broadening that increases with binding energies). The final states of the Mn $2p$ core-level photoemission are given by the linear combinations of the $\underline{2p}d^5$, $\underline{2p}d^6\underline{L}$, . . . , $\underline{2p}d^{10}\underline{L}^5$ configurations, where $\underline{2p}$ represents a Mn $2p$ core hole. In the bottom panels of Fig. 1, the calculated spectrum is decomposed into the $\underline{2p}d^5$ and $\underline{2p}d^6\underline{L}$ components of the final-state configurations. The relative intensity and energy of the satellite to the main peak are mainly determined by $\Delta - Q$ and $(pd\sigma)$. Here, Q is the averaged Coulomb interaction between the Mn $3d$ electron and the Mn $2p$ core hole and the U/Q ratio is fixed at 0.8. The satellite structure for Mn $2p_{3/2}$ is well reproduced with $\Delta=6.5\pm1.5$ eV, $\Delta - Q = 0.0 \pm 0.5$ eV, and $(pd\sigma) = -1.6 \pm 0.1$ eV. The obtained U and Q values are 5.2 ± 1.0 eV and 6.5 ± 1.5 eV, respectively.

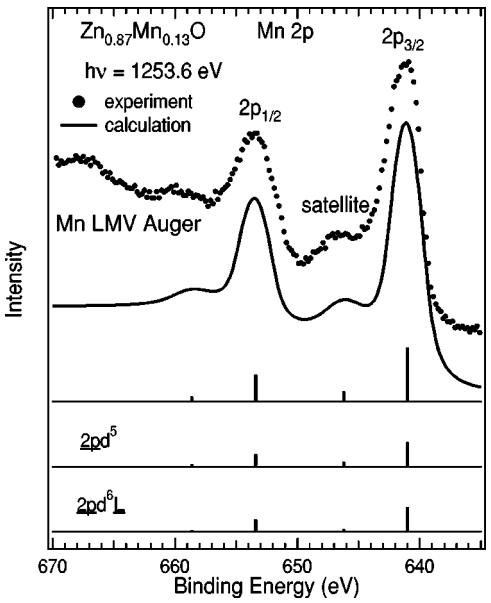

FIG. 1. Mn $2p$ core-level photoemission spectrum of $Zn_{0.87}Mn_{0.13}O$ (dots) and its CI cluster-model analysis (solid curve). In the bottom panels, the calculated spectrum is decomposed into the $\underline{2p}d^5$ and $\underline{2p}d^6\underline{L}$ components of the final-state configurations.

In order to demonstrate the chemical trend in the chalcogenide-based and oxide-based DMS, the Mn $2p$ core-level spectrum of $Zn_{1-x}Mn_xO$ is compared with those of $Zn_{1-x}Mn_xS$ and MnO (Ref. 10) in Fig. 2. The intensity of the satellite structure is enhanced in $Zn_{1-x}Mn_xS$ compared to those in $Zn_{1-x}Mn_xO$ and MnO. We have analyzed the Mn $2p$ spectra using the octahedral MnY_6 cluster model for MnO and the tetrahedral MnY_4 cluster model for $Zn_{1-x}Mn_xO$ and $Zn_{1-x}Mn_xS$. The calculated results are shown by the solid curves in Fig. 2. The satellite structure for Mn $2p_{3/2}$ is well reproduced with $\Delta=6.0\pm1.5$ eV for MnO and with $\Delta=2.5\pm1.0$ eV for $Zn_{1-x}Mn_xS$. Δ of $Zn_{1-x}Mn_xO$ is similar to that of MnO and is much larger than that of $Zn_{1-x}Mn_xS$, indicating that Δ is mainly determined by the electronegativity of the anions. The U value for MnO is 6.0 ± 1.0 eV and that for $Zn_{1-x}Mn_xS$ is 4.4 ± 1.0 eV, which may be attributed to the higher polarizability of the S ions than that of the O ion.

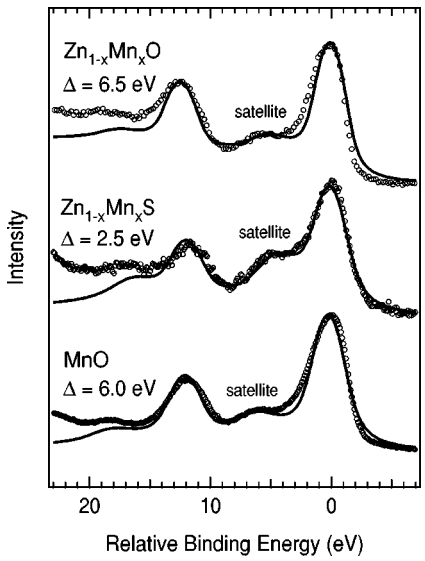

FIG. 2. Mn $2p$ core-level photoemission spectrum of $Zn_{1-x}Mn_xO$ is compared with those of $Zn_{1-x}Mn_xS$ and MnO (Ref. 10) (open circles). The calculated results are shown by the solid curves.

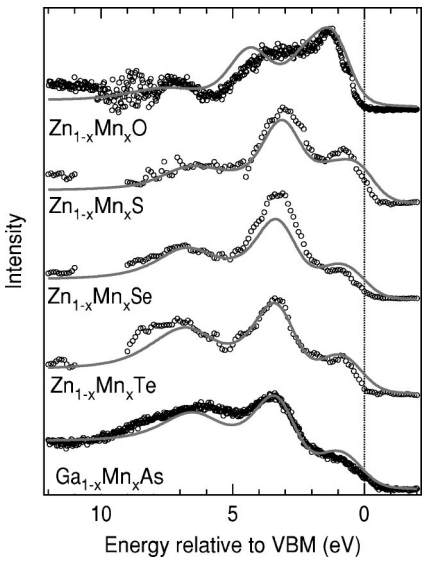

FIG. 4. Mn $3d$-derived photoemission spectra of $Zn_{0.93}Mn_{0.07}O$ (50.5 eV−49 eV difference spectrum, open circles) compared with those of $Zn_{0.81}Mn_{0.19}S$, $Zn_{0.81}Mn_{0.19}Se$, $Zn_{0.68}Mn_{0.32}Te$, (Ref. 15), and $Ga_{0.93}Mn_{0.07}As$ (Ref. 12). Binding energies are referenced to VBM of the host semiconductors. The calculated results are shown by the solid curves.

B. Valence-band photoemission

Figure 3 shows valence-band photoemission spectra of $Zn_{1-x}Mn_xO$ with $x=0.07$ taken at various photon energies in the Mn $3p\rightarrow 3d$ core-excitation region. The binding energies are referenced to VBM. In Fig. 3, structures a, b, and c are located at ~2.5 eV, 6 eV, and 9 eV and mainly have character of nonbonding O $2p$, O $2p$ hybridized with Zn $4s$, and Zn $3d$, respectively.[16] Resonant photoemission[11] is a powerful technique to extract the Mn $3d$-derived photoemission spectrum. The Mn $3p\rightarrow 3d$ resonant photoemission measurement has been performed for other DMS such as $Ga_{1-x}Mn_xAs$,[12] $Cd_{1-x}Mn_xY$,[13,14] and $Zn_{1-x}Mn_xY$ (Y=S, Se, and Te).[15]

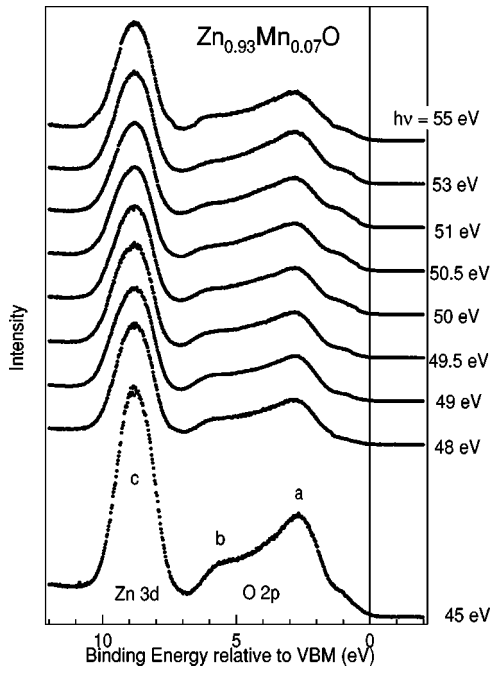

FIG. 3. A series of valence-band photoemission spectra of $Zn_{0.93}Mn_{0.07}O$ using photon energies in the Mn $3p$ core-excitation region.

The Mn $3d$-derived spectrum of $Zn_{0.93}Mn_{0.07}O$ is compared with those of other II-VI-based[15] and III-V-based[12] DMS in Fig. 4. The Mn $3d$-derived spectrum of $Zn_{0.93}Mn_{0.07}O$ has been obtained by subtracting the off-resonance spectrum ($h\nu=49$ eV) from the on-resonance one ($h\nu=50.5$ eV) that are normalized to the intensity of the Zn $3d$ peak. The Mn $3d$-derived spectra of the chalcogenide-based II-VI DMS commonly have the three characteristic features: the shoulder at ~1 eV, the main peak at ~3.5 eV, and the high binding-energy satellite at ~7 eV. The CI cluster-model calculations for II-VI- and III-V-based DMS can explain the shoulder, the main peak and the satellite structure as shown by the solid curves in Fig. 4. The shoulder and the main peak mainly consist of $d^5\underline{L}$ final states and the satellite is derived from the unscreened d^4 final states. The Mn $3d$-derived spectrum for $Zn_{1-x}Mn_xO$ looks different from the chalcogenide-based DMS. However, one can still recognize the chemical trend in the whole series of materials. In going from ZnTe to ZnO, the intensity of the structure at ~1 eV increases compared to the structure at ~7 eV. In particular, these changes are drastic between ZnS and ZnO because of the large electronegativity jump between S and O.

The Mn $3d$-derived spectrum of $Zn_{1-x}Mn_xO$ can be explained by the CI cluster-model calculation with $\Delta=6.5\pm1.0$ eV, $U=5.2\pm1.0$ eV, and $(pd\sigma)=-1.6\pm0.2$ eV. In principle, Δ and U values for the valence-band spectrum would be different from those for the Mn $2p$ core-level spectrum because the number of d and core electrons is different in the

TABLE I. Parameters used to calculate the valence-band photoemission spectra and estimated p-d exchange constant $N\beta$ for Mn^{2+} impurities in ZnO, ZnS, ZnSe, ZnTe, and GaAs (in eV).

	Δ	U	$(pd\sigma)$	$N\beta$
$Zn_{1-x}Mn_xO$	6.5	5.2	−1.6	−2.7
$Zn_{1-x}Mn_xS$	3.0	4.0	−1.3	−1.3
$Zn_{1-x}Mn_xSe$	2.0	4.0	−1.1	−1.0
$Zn_{1-x}Mn_xTe$	1.5	4.0	−1.0	−0.9
$Ga_{1-x}Mn_xAs$	1.5	3.5	−1.0	−0.9

final states of the two spectra. However, in the present analyses, the Δ and U values are consistent between the valence-band and Mn $2p$ core-level spectra within the error bars. Probably, the difference due to the final-state effect is smaller than the error bar of the fitting procedure. Although the agreement between theory and experiment is not perfect and is semiquantitative, it is sufficient to extract chemical trends in the electronic-structure parameters of II-VI- and III-V-based DMS. The obtained parameter sets for Mn impurities in the various II-VI- and III-V semiconductors are summarized in Table I.[17] The parameters for ZnO and ZnS are consistent with those obtained from the Mn $2p$ core-level spectra. In going from ZnO to GaAs, the charge-transfer energy Δ decreases as the electronegativity of the ligand decreases. The transfer integral $(pd\sigma)$ also decreases as the distance between the transition-metal cation and the ligand anions increases. The drastic change of Δ between ZnS and ZnO can be attributed to the electronegativity jump between S and O.

C. d-d transition

The d-d transition of the Mn^{2+} impurity in wide-gap semiconductors is of particular importance in the light of technological applications. The ground state of the Mn^{2+} impurity is ${}^6A_1$. The d-d transition energy from ${}^6A_1$ to the lowest excited terms ${}^4T_1$, ${}^4T_2$, ${}^4E$, and ${}^4A_1$ are calculated using the cluster model and are listed in Table II for ZnO, ZnS, ZnSe, ZnTe, and GaAs hosts. These excited terms originate from the ${}^4G$ term of the free d^5 ion. For Mn^{2+} in ZnO, the d-d transitions from the ${}^6A_1$ ground state to ${}^4T_1$, ${}^4T_2$, ${}^4E$, and ${}^4A_1$ excited states are calculated to be 2.55, 2.85, 2.97, and 2.99 eV, respectively. In going from ZnO to GaAs, the p-d hybridization increases and, consequently, these excitation energies become smaller. For Mn^{2+} in ZnS and ZnSe, the calculated values agree with the experimental results reasonably well.[8] It is known that the intensity of ${}^4T_1$ is very weak compared to those of ${}^4T_2$, ${}^4E$, and ${}^4A_1$ in the tetrahedral coordination geometry. Therefore, it is reasonable to assign the broad absorption band around 3 eV observed in the $Zn_{1-x}Mn_xO$ thin film[4] to the d-d transitions from ${}^6A_1$ to ${}^4T_2$, ${}^4E$, and ${}^4A_1$.

TABLE II. Calculated energy levels of ${}^4T_1$, ${}^4T_2$, ${}^4E$, and ${}^4A_1$ for Mn^{2+} impurities in ZnO, ZnS, ZnSe, ZnTe, and GaAs (in eV).

	${}^4T_1$	${}^4T_2$	${}^4E$	${}^4A_1$
$Zn_{1-x}Mn_xO$	2.55	2.85	2.97	2.99
$Zn_{1-x}Mn_xS$	2.31	2.57	2.70	2.76
$Zn_{1-x}Mn_xSe$	2.27	2.48	2.59	2.67
$Zn_{1-x}Mn_xTe$	2.22	2.41	2.51	2.61
$Ga_{1-x}Mn_xAs$	2.19	2.39	2.49	2.59

D. p-d exchange constant

The exchange interaction between the p holes in the valence band and the d electrons is mainly derived from the p-d hybridization.[2,18] Especially at the Γ point, the top of the valence band is constructed purely from the anion p orbitals that can only hybridize with the d orbitals of t_2 symmetry. In the CI picture, the lowest $d^n\underline{L}_0$ configuration, where $\underline{L}_0$ denotes a hole at VBM hybridizes with the d^{n-1} and $d^{n+1}\underline{L}_0^2$ configurations. The energy difference between the lowest terms of $d^n\underline{L}_0$ and $d^{n+1}\underline{L}_0^2$ is given by $\delta_{\rm eff}\equiv\Delta_{\rm eff}-W_V/2$. Here, W_V is the width of the host valence band contributing to the hybridization term and is fixed at 2 eV because the upper 2 eV of the valence band mainly contributes to the hybridization term although the total width of the valence band is 4–5 eV. The lowest term of d^{n-1} is by $U_{\rm eff}-\delta_{\rm eff}$ higher than that of $d^n\underline{L}_0$. Using the electronic-structure parameters $\Delta, U, (pd\sigma)$ obtained from the CI calculation for the photoemission spectra, we can calculate $N\beta$ for the $3d$ transition-metal impurities in the second order of perturbation with respect to the hybridization term.

The t_2 orbitals are half filled in Mn^{2+}. When a hole is located at VBM with spin parallel to the Mn spin (namely, an electron is located at VBM with spin antiparallel to the Mn spin), the t_2 electron can be transferred into the unoccupied valence-band state with parallel spin and the valence-band electron with antiparallel spin can be transferred into the unoccupied t_2 states. The intermediate states thus produced contribute to the kinetic exchange interaction between the carrier and Mn spins. On the other hand, when a hole is located at VBM with spin antiparallel to the Mn spin, there is no intermediate state available. Therefore, the p-d exchange interaction between the hole carriers and the Mn spins is antiferromagnetic. The exchange constant $N\beta$ is given by

$$N\beta=-\frac{16}{S}\left(\frac{1}{-\delta_{\rm eff}+U_{\rm eff}}+\frac{1}{\delta_{\rm eff}}\right)\left[\frac{1}{3}(pd\sigma)-\frac{2\sqrt{3}}{9}(pd\pi)\right]^2 \tag{1}$$

for the Mn^{2+} impurity.[18–20] Here, $U_{\rm eff}=u+4j$, $u=A+4B+3C$, $j=5B/2+C$, and $A=U+(14B-7C)/9$. The magnitude of the local spin S is 5/2. The estimated $N\beta$ for Mn^{2+} in ZnO, ZnS, ZnSe, ZnTe, and GaAs are listed in Table I. Interestingly, the magnitude of $N\beta$ of $Zn_{1-x}Mn_xO$ is predicted to be much larger than that of $Ga_{1-x}Mn_xAs$ although the p-d hybridization in the ground state is much weaker in $Zn_{1-x}Mn_xO$ than in $Ga_{1-x}Mn_xAs$. The origin of the large $|N\beta|$ in $Zn_{1-x}Mn_xO$ is the strong p-d hybridization in the ionization states. Since $\Delta_{\rm eff}$ is as large as $U_{\rm eff}$ in $Zn_{1-x}Mn_xO$, the contribution of the first term in Eq. (1) becomes substan-

tial and gives the large $|N\beta|$. The present result is consistent with the theoretical study by Dietl *et al.*, which predicts that the Curie temperature of $Zn_{1-x}Mn_xO$ reaches 300 K while that of $Ga_{1-x}Mn_xAs$ is about 100 K.[21]

V. CONCLUSION

In conclusion, we have investigated the electronic structure of $Zn_{1-x}Mn_xO$ using photoemission spectroscopy and CI cluster-model analysis. The CI calculation using the MnO_4 cluster model can explain the Mn $2p$ and valence-band photoemission spectra as well as the d-d optical absorption spectra. The present CI calculation predicts that the p-d exchange constant $N\beta$ in $Zn_{1-x}Mn_xO$ is -2.7 eV and that its magnitude is much larger than that in $Ga_{1-x}Mn_xAs$. Application of the CI method with a more realistic model to a wider range of diluted magnetic semiconductors remains to be made in future.

ACKNOWLEDGMENTS

The authors would like to thank K. Ando, A. K. Bhattacharjee, and D. D. Sarma for useful and enlightening discussions. The authors would like to thank J. Okabayashi, T. Kinoshita, and A. Harasawa for valuable technical support in the measurements. This work was supported by a Grant-in-Aid for Scientific Research in the priority area ''Spin Controlled Semiconductor Nanostructures'' and the Special Coordination Fund for the Promotion of Science and Technology from the Ministry of Education, Culture, Sports, and Science and Technology of Japan. The experiment at Photon Factory was approved by the Photon Factory Program Advisory Committee (Proposal No. 99G140).

[1] A. Zunger, in *Solid State Physics*, edited by H. Ehrenreich and D. Turnball (Academic, New York, 1980), Vol. 39; H. Katayama-Yoshida and A. Zunger, Phys. Rev. B **33**, 2961 (1986).
[2] J.K. Furdyna, J. Appl. Phys. **64**, R29 (1988); *Diluted Magnetic Semiconductors*, edited by J.K. Furudyna and J. Kossut, Semiconductors and Semimetals (Academic, New York, 1988), Vol. 25.
[3] H. Ohno, Science **281**, 951 (1998); J. Magn. J. Magn. Magn. Mater. **200**, 110 (1999).
[4] T. Fukumura, Zhengwu Jin, A. Ohtomo, H. Koinuma, and M. Kawasaki, Appl. Phys. Lett. **75**, 3366 (1999).
[5] K. Sato and H. Katayama-Yoshida, Jpn. J. Appl. Phys., Part 2 **39**, L555 (2000).
[6] L. Ley, R.A. Pollak, F.R. McFeely, S.P. Kowalczyk, and D.A. Shirley, Phys. Rev. B **9**, 600 (1974).
[7] R.R. Gay, M.H. Nodine, V.E. Henrich, H.J. Zeiger, and E.I. Solomon, J. Am. Chem. Soc. **102**, 6752 (1980).
[8] T. Mizokawa and A. Fujimori, Phys. Rev. B **48**, 14 150 (1993); *ibid.* **56**, 6669 (1997).
[9] W.A. Harrison, *Electronic Structure and the Properties of Solids* (Dover, New York, 1989).
[10] A.E. Bocquet, T. Mizokawa, T. Saitoh, H. Namatame, and A. Fujimori, Phys. Rev. B **46**, 3771 (1992).
[11] L.C. Davis, J. Appl. Phys. **59**, R25 (1986).
[12] J. Okabayashi, A. Kimura, T. Mizokawa, A. Fujimori, T. Hayashi, and M. Tanaka, Phys. Rev. B **59**, R2486 (1999).
[13] M. Taniguchi, A. Fujimori, M. Fujisawa, T. Mori, I. Souma, and Y. Oka, Solid State Commun. **62**, 431 (1987).
[14] L. Ley, M. Taniguchi, J. Ghijsen, R.L. Johnson, and A. Fujimori, Phys. Rev. B **35**, 2839 (1987).
[15] R. Weidemann, H.-E. Gumlich, M. Kupsch, H.-U. Middelmann, and U. Becker, Phys. Rev. B **45**, 1172 (1992).
[16] W. Ranke, Solid State Commun. **19**, 685 (1976).
[17] In the present paper, we analyzed the photoemission spectra of $Zn_{1-x}Mn_xSe$ and $Zn_{1-x}Mn_xTe$ reported by Weidemann *et al.* (Ref. 15). The parameters for $Zn_{1-x}Mn_xSe$ and $Zn_{1-x}Mn_xTe$ are slightly different from those obtainted previously (Ref. 8) for $Cd_{1-x}Mn_xSe$ and $Cd_{1-x}Mn_xTe$.
[18] B.E. Larson, K.C. Hass, H. Ehrenreich, and A.E. Carlsson, Phys. Rev. B **37**, 4137 (1988); K.C. Hass, in *Semimagnetic Semiconductors and Diluted Magnetic Semiconductors*, edited by M. Averous and M. Balkanski (Plenum, New York, 1991), p. 59.
[19] A.K. Bhattacharjee, Phys. Rev. B **46**, 5266 (1992).
[20] J. Blinowski and P. Kacman, Phys. Rev. B **46**, 12 298 (1992).
[21] T. Dietl, H. Ohno, F. Matsukura, J. Cibert, and D. Ferrand, Science **287**, 1019 (2000).